HAL
open science

The transmission spectrum of Earth-size transiting planets

David Ehrenreich, Giovanna Tinetti, Alain Lecavelier Des Etangs, Alfred Vidal-Madjar, Franck Selsis

To cite this version:

David Ehrenreich, Giovanna Tinetti, Alain Lecavelier Des Etangs, Alfred Vidal-Madjar, Franck Selsis. The transmission spectrum of Earth-size transiting planets. 2005. hal-00009612

HAL Id: hal-00009612

https://hal.science/hal-00009612

Preprint submitted on 7 Oct 2005

HAL is a multi-disciplinary open access archive for the deposit and dissemination of scientific research documents, whether they are published or not. The documents may come from teaching and research institutions in France or abroad, or from public or private research centers.

L'archive ouverte pluridisciplinaire **HAL**, est destinée au dépôt et à la diffusion de documents scientifiques de niveau recherche, publiés ou non, émanant des établissements d'enseignement et de recherche français ou étrangers, des laboratoires publics ou privés.

Astronomy & Astrophysics manuscript no. Ehrenreich2005˙preprint.hyper16096 October 7, 2005
(DOI: will be inserted by hand later)

The transmission spectrum of Earth-size transiting planets

D. Ehrenreich[1], G. Tinetti[2], A. Lecavelier des Etangs[1], A. Vidal-Madjar[1], and F. Selsis[3]

[1] Institut d'Astrophysique de Paris, CNRS (UMR 7095) – Université Pierre & Marie Curie, 98 bis, boulevard Arago 75014 Paris, France, e-mail: ehrenreich@iap.fr
[2] NASA Astrobiology Institute, California Institute of Technology, IPAC, MS 220-6, 1 200 E. California, Pasadena, 91125 (CA), USA
[3] Centre de Recherche Astronomique de Lyon, École Normale Supérieure, 47, allée d'Italie 69364 Lyon Cedex 7, France

Received / Accepted

Abstract. A variety of terrestrial planets with different physical parameters and exotic atmospheres might plausibly exist outside our Solar System, waiting to be detected by the next generation of space-exploration missions. Some of these planets might transit their parent star. We present here the first study of atmospheric signatures of transiting Earth-size exoplanets. We focus on a limited number of significant examples, for which we discuss the detectability of some of the possible molecules present in their atmospheres, such as water (H_2O), carbon dioxide (CO_2), ozone (O_3) or molecular oxygen (O_2). To this purpose, we developed a model to simulate transmission spectra of Earth-size exoplanets from the ultraviolet (UV) to the near infrared (NIR). According to our calculations, the signatures of planetary atmospheres represent an absorption of a few parts-per-million (ppm) in the stellar flux. The atmospheres of a few Earth-like planets can be detected with a 30–40 m telescope. The detection of the extensive atmospheres of tens of small satellites of giant exoplanets and hundreds of hypothetical ocean-planets can be achieved with 20–30 m and 10–20 m instruments, respectively, provided all these planets are frequent and they are efficiently surveyed. We also found that planets around K stars are favored, mainly because these stars are more numerous and they are smaller compared to G or F stars. While not addressed in this study, limitations might come from the stellar photometric micro-variability.

ccsd-00009612, version 1 - 7 Oct 2005

1. Introduction

The Earth is the only known example of a life-hosting world, even though terrestrial exoplanets have been searched for since the discovery of the first Earth-mass exoplanets by Wolszczan & Frail (1992). However, planets similar to the Earth, Venus or Mars, in size, density or orbital parameters are still beyond the reach of the present capabilities for planet detection around normal stars.

Until now, mostly giant exoplanets have been discovered. Remarkable progresses have been made recently with the discovery of planets in the mass range of 14 to 21 Earth masses (14 to 21 $M_\oplus$, see McArthur et al. 2004; Santos et al. 2004), and most recently a $\sim$7.5 $M_\oplus$ planet orbiting GJ 876 (Rivera et al. 2005). We may speculate, then, that smaller planets with sizes down to that of the Earth might be observed in a near future. Among the 161 planets[1] detected so far, eight have been discovered or re-discovered as they were transiting their parent star, producing a photometric occultation. The last transiting planet identified is a Saturn-mass planet orbiting HD 149 026, a bright $V = 8.15$ G0 IV star (Sato et al. 2005). The first discovered transiting giant exoplanet, HD 209 458b (Henry et al. 2000; Charbonneau et al. 2000; Mazeh et al. 2000), is the object of intense investigations dedicated to characterizing its hot atmosphere.

Probing planetary atmospheres by stellar occultations is an effective method used for a lot of planets and their satellites in the Solar System, from Venus to Charon (see, e.g., Elliot & Olkin 1996). With this technique, we can observe the thin atmospheric ring surrounding the optically thick disk of the planet: the limb. In the case of giant exoplanets, though, the star is only partially occulted (1.6% for the transiting planet HD 209 458b). The spectrum of the star light transmitted and filtered by the lower and thick giant exoplanet atmosphere consequently presents extremely weak absorption features (from 10^{-3} to 10^{-4}, see Seager & Sasselov 2000; Hubbard et al. 2001; Brown 2001).

Despite the difficulties, such dim signatures were detected: Charbonneau et al. (2002) measured the

Send offprint requests to: D. Ehrenreich

[1] From J. Schneider's Extrasolar Planets Encyclopædia at vo.obspm.fr/exoplanetes/encyclo/encycl.html. See also the web page of the IAU Working Group on Extrasolar Planets at www.ciw.edu/boss/IAU/div3/wgesp.

lower atmosphere of HD 209 458b as they detected a $(2.32 \pm 0.57) \cdot 10^{-4}$ photometric diminution in the sodium doublet line of the parent star at 589.3 nm. However its upper atmosphere, which extends up to several planet radii, shows even larger signatures. Vidal-Madjar et al. (2003, 2004) observed a $15 \pm 4\%$ absorption in the Lyman α (Ly_α) emission line of HD 209 458 at 121.57 nm as well as absorptions from atomic carbon ($7.5 \pm 3.5\%$) and oxygen ($13 \pm 4.5\%$) in the upper atmosphere. In this work, we will discuss the possibility to detect and to characterize the lower atmospheres of exoplanets using signatures comparable in origin to the one detected by Charbonneau et al. (2002).

The idea is to extend the use of transmission spectroscopy to hypothetical Earth-size planets. We estimate that these exoplanets present at least two orders of magnitude less signal than gaseous giants, as the transit of the planet itself would have a dimming of $\sim 10^{-5}$ (the transit depth, $\Delta F/F$, where F is the stellar flux, can be expressed as $(R_P/R_\star)^2$, with R_P and $R_\star$ standing for the radii of the planet and the star, respectively). The atmospheres of Earth-size exoplanets should span over $\sim$100-km height without considering potential upper atmospheres. Depending on their transparency – which would give an equivalent optically thick layer of $\sim$10 km – the expected occultations caused by atmospheric absorptions should be $\sim 10^{-7}$ to $\sim 10^{-6}$.

Earth-size planets are probably the most challenging objects to detect with transmission spectroscopy. The orders of magnitude given above, in fact, raise many questions: is it realistic to seek for possible features that dim, with an instrumentation that might or might not be available in a near future? What are the strongest signatures we should expect? What kind of planet could be the best candidate to look at?

We have developed a one-dimensional model of transmission at the limb to give quantitative answers to these questions. Since we use the stellar light to explore the planetary atmospheres, we chose to focus on the wavelength range where the largest number of photons is available, i.e., between 200 and 2 000 nm. The model is described in Sect. 2. The detectability of the selected atmospheres depends on the signal-to-noise ratio (S/N) achievable with a space telescope spectrograph. The constraints on idealized observations and the method we used to calculate their S/N, are described in Sect. 3. Finally, the results for the specified cases are given and discussed in Sect. 4.

2. Model description

2.1. Geometric description of the model

The general geometry of a transiting system is described by Brown (2001). In the present work we consider a non-transient occultation for the 'in transit' phase, with a null phase configuration (configuration 2 in Brown's Fig. 1), that is, the planet is centered in the line of sight with respect to the star. This configuration both maximizes the area of the atmosphere that is filtering the stellar light and minimizes any effects linked to the stellar limb darkening (Seager & Sasselov 2000).

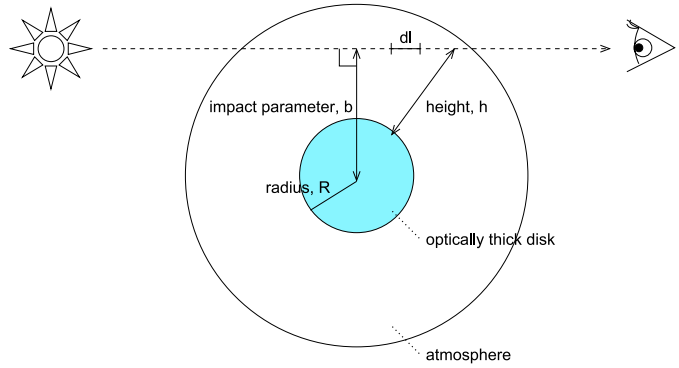

Fig. 1. Sketch of the transmission of the stellar light through the planetary limb. The planet itself, i.e. the 'solid' disk (in grey) is optically thick at all wavelengths. The quantity dl is the elemental length along the line of sight. In the calculation, we prefer to use the height h instead of l. The scale in the figure has been distorted for clarity.

The stellar light is filtered through the atmospheric limb of the planet, as sketched in Fig. 1. In the following we detail the integration of the atmospheric opacity along a stellar light path (or cord) through the limb of the planet.

2.1.1. Opacity along the line of sight

We calculate the total opacity of the model atmosphere, τ_λ, along a cord, parallel to the line of sight, as the sum of the opacity of each species i present in the atmosphere, $\tau_\lambda = \sum_i \tau_{\lambda,i}$. We can calculate the opacity along the cord as a function of its impact parameter, b:

$$\tau_{\lambda,i}(b) = 2 \int_0^{+\infty} A_{\lambda,i} \rho_i(h) \mathrm{d}l, \tag{1}$$

where $A_{\lambda,i}$ is the absorption coefficient for the species i at the wavelength λ, expressed in $\mathrm{cm}^2\,\mathrm{g}^{-1}$, and $\rho_i(h)$ is the mass density in $\mathrm{g\,cm}^{-3}$ of the species i at an altitude h in the atmosphere.

Now, re-expressing Eq. 1 as a function of the height $z = h + R_P$, with R_P being the planet radius, we obtain:

$$\tau_{\lambda,i}(b) = 2 \int_b^{b_{\max}} A_{\lambda,i} \rho_i(z - R_P) \frac{z \mathrm{d}z}{\sqrt{z^2 - b^2}}, \tag{2}$$

where $b_{\max}$ is the height of the higher atmospheric level we are considering. The method to estimate $b_{\max}$ is presented in Sect. 2.2.3.

2.1.2. Spectrum ratio

Consider the stellar flux received by the observer during the planetary transit to be F_{in}, and the flux received when the planet is not occulting the star to be F_{out}. Brown

(2001) defined $\Re$ to be the ratio between those two quantities, and $\Re'$ (the so-called spectrum ratio) as $\Re' = \Re - 1$. Here, $\Re'$ is the sum of two distinct types of occultations:

- The occultation by the 'solid' surface of the planet, optically thick at all wavelengths. Projected along the line of sight, this is a disk of radius R_P and the occultation depth is simply $(R_P/R_\star)^2$.
- The wavelength-dependent occultation by the thin ring of gaseous components that surrounds the planetary disk, which can be expressed as $\Sigma_\lambda/(\pi R_\star^2)$. The area, Σ_λ, is the atmospheric equivalent surface of absorption and may be calculated as:

$$\Sigma_\lambda = \int_{R_P}^{b_{\max}} 2\pi b \mathrm{d}b \left[1 - \mathrm{e}^{-\tau_\lambda(b)}\right]. \quad (3)$$

The resulting spectrum ratio is:

$$\Re'(\lambda) = -\frac{\Sigma_\lambda + \pi R_P^2}{\pi R_\star^2}. \quad (4)$$

Note that $\Re' < 0$.

2.2. Description of the atmospheric profiles

Along a single cord, stellar photons are crossing several levels of the spherically stratified atmosphere. We generate an atmospheric model using the vertical profiles from Tinetti et al. (2005a, 2005b) and Fishbein et al. (2003) for the Earth and from the Venus International Reference Atmosphere (VIRA, Kliore et al. 1985) for Venus. These atmospheric data include the profiles of pressure, p, temperature, T, and various mixing ratios, Y. The atmospheres are initially sampled in 50 levels, ranging from the ground level to an altitude of about 80 km for the Earth and about 50 km for Venus. Both profiles stop below the homopause, so we assume hydrostatic equilibrium for the vertical pressure gradient.

A useful quantity to describe atmospheres in hydrostatic equilibrium is the scale height, H, i.e. the height above which the pressure decreases by a factor e. The scale height explicitly depends on the temperature, as $H = k\mathcal{N}_A T/(\mu g)$, where k and $\mathcal{N}_A$ are the Boltzmann's and Avogadro's constants while μ is the mean molar mass of the atmospheric gas. Since g is the acceleration due to gravity, H also implicitly depends on the radius and the density of the planet[2]. Consequently, less dense objects are likely to have more extensive atmospheres, hence they are easier to detect (Brown 2001).

Density and size of planets are therefore key parameters for the present work. In order to estimate their influence, we test a set of different planetary types ranging from the Titan-like giant planet's satellite ($\rho_P \approx 2\,\mathrm{g\,cm^{-3}}$, $R_P \approx 0.5$ Earth radius – 0.5 $\mathrm{R_\oplus}$) to the 'super-Earth' object ($\rho_P \approx 6\,\mathrm{g\,cm^{-3}}$, $R_P \approx 2\,\mathrm{R_\oplus}$). For the physical properties of plausible, theoretically predicted planets such as a 'super-Earth', we use the mass-radius relation model from Dubois (2004) and from Sotin et al. (2005). Our atmospheric model allows the re-scaling of vertical profiles depending on the acceleration due to gravity of the planet and the atmospheric pressure at the reference level.

[2] To avoid confusion between the density of the atmosphere and the mean density of the planet, the latter is denoted ρ_P

2.2.1. Molecular composition of the atmosphere

Our simplified atmospheric profiles contain only the species that may produce interesting spectral signatures in the chosen wavelength range (0.2 to 2 μm), viz., water vapor (H_2O), carbon dioxide (CO_2), ozone (O_3) and molecular oxygen (O_2). Molecular nitrogen (N_2) has also been considered, though lacking marked electronic transitions from the UV to the near IR. Nevertheless, it is a major species in Earth's atmosphere and it has a detectable signature via Rayleigh scattering at short wavelengths.

We consider three types of atmospheres: (A) N_2/O_2-rich, (B) CO_2-rich and (C) N_2/H_2O-rich cases. The first two types can be associated with existing planetary atmospheres, respectively Earth and Venus. The last type (C) could correspond to the atmosphere of an Earth-mass volatile-rich planet such as an 'ocean-planet' described by Léger et al. (2004). The basis for building a 'toy model' of an H_2O-rich atmosphere are found in Léger et al. (2004) and Ehrenreich et al. (2005b, see Sect. 2.2.5).

Vertical gradients in the chemical composition and temperature of each of these atmospheres are plotted in Fig. 2 (N_2/O_2-rich), Fig. 3 (CO_2-rich) and Fig. 4 (N_2/H_2O-rich). Table 1 summarizes the mean chemical compositions of these model atmospheres.

2.2.2. Temperature profiles

As mentioned above, we use Earth and Venus vertical temperature profiles as prototype for N_2/O_2-rich and CO_2-rich atmospheres (see Sect. 2.4). Moreover we assume an isothermal profile in the thermosphere, instead of the real one. This is an arbitrary, but conservative choice, since the temperature should on the contrary rise in the thermosphere enhancing the atmosphere's detectability (see Sect. 4.2.2).

2.2.3. Upper limit of the atmosphere

We set the profiles to extend up to a critical height $b_{\max}$ from the centre of the planet, or $h_{\max}$ from the surface ($b_{\max} = R_P + h_{\max}$). This limit corresponds to the altitude above which the molecular species we considered (H_2O, O_3, CO_2, O_2) are likely to be destroyed or modified either by photo-dissociating or ionizing radiations, such as Ly_α or extreme-UV (EUV).

Therefore, the critical height corresponds to the mesopause on Earth (at $\approx$ 85 km). The column density of the terrestrial atmosphere above that altitude, $\mathcal{N}_{\geq 85\,\mathrm{km}}$, is sufficient to absorb all Ly_α flux. In fact, as the number density of the atmospheric gas, $n(h)$, de-

Type	μ (g mol^{-1})	Y_{N_2}(%)	Y_{H_2O} (%)	Y_{CO_2} (%)	Y_{O_2} (%)	Y_{O_3} (%)	Used for models
N_2/O_2-rich	28.8	78	0.3	0.03	21	$< 10^{-3*}$	A1, A2, A3
CO_2-rich	43.3	4	$3 \cdot 10^{-4}$	95	0	0	B1, B2, B3
N_2/H_2O-rich	28.7	80	10	10	0	0	C1, C2, C3

Table 1. Mean volume mixing ratio of atmospheric absorbers for the different types of model atmospheres considered. (*) Ozone is only present in model A1.

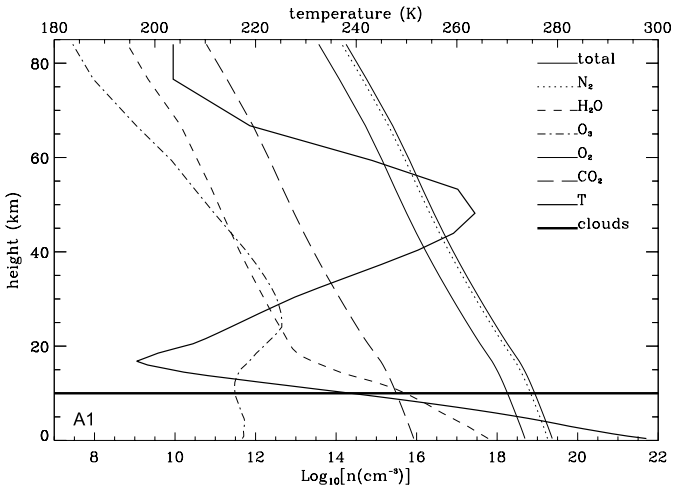

Fig. 2. Atmospheric profiles, A1. The plot shows the total number density profile (thin solid line) of the atmosphere in cm^{-3}, and that of the five species included in our model, namely, N_2 (dotted line), O_2(dash-dot-dot-dotted line), H_2O (dashed line), CO_2 (long-dashed line) and O_3 (dash-dotted line). Temperature (thick line up to 80 km) and mixing ratios of the different species are those of Earth. Temperature is assumed to be constant above that height. The thickest horizontal line shows the position of the cloud layer.

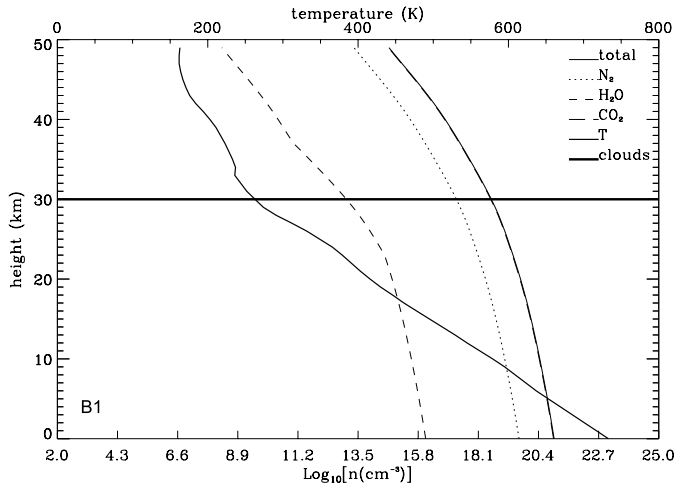

Fig. 3. Atmospheric profiles, B1. The legend is identical to that in Fig. 2. The temperature profile and mixing ratios are that of Venus. The temperature is considered to be constant above 50 km. Carbon dioxide is barely visible because it is by far the major constituent so its line is superimposed with that of the total density.

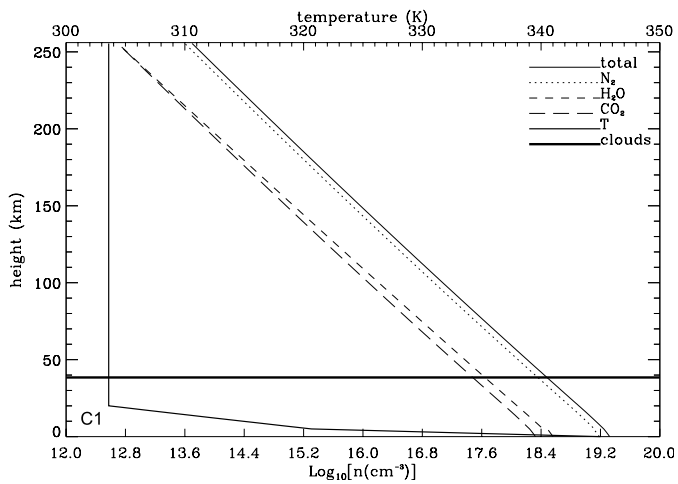

Fig. 4. Atmospheric profiles, C1. Same legend as in Fig. 2 and Fig. 3. The temperature profile follows a dry adiabat in the first 10 km of the atmosphere, until the point where $e \geq e_{\rm sat}$. Next, it follows a steeper saturated adiabat up to 20 km high. The temperature gradient is arbitrarily set to be isothermal above this point. The cloud top (thickest line) is one scale height above the higher point where $e \geq e_{\rm sat}$. For reasons detailed in the text (see Sect. 2.2.5), this point corresponds to the level where the temperature gradient becomes isothermal.

creases exponentially with height, we can simply consider $\mathcal{N}_{\geq 85\,\rm km} \propto n_{85\,\rm km} \cdot H_{85\,\rm km}$, where $n_{85\,\rm km}$ and $H_{85\ \rm km}$ are the density and the scale height of the terrestrial atmosphere at 85 km, respectively.

Similarly, we set the upper limit of a given atmosphere, $h_{\rm max}$, to the altitude below which the photodissociating photons are absorbed. We assume that $h_{\rm max}$ is the altitude where the column density equals that of the terrestrial atmosphere at 85 km, that is $n_{h_{\rm max}} \cdot H_{h_{\rm max}} = (n_{85\,\rm km})_\oplus \cdot (H_{85\,\rm km})_\oplus$. We determine $h_{\rm max}$ by scaling this equation.

Values of $h_{\rm max}$ for the different models are given in Table 2. Similarly to neutral elements absorbing light below $h_{\rm max}$, it is likely that ionized elements are absorbing light above this limit, though we do not include this effect in the model.

2.2.4. Presence of clouds

In the wavelength range of interest, the surface of Venus is almost completely hidden by clouds. Therefore, it seems reasonable to model these types of clouds to a first order

approximation by assuming that they act as an optically thick layer at a given altitude. As a result, clouds effectively increase the apparent radius of the planet and the transiting spectrum gives information only about atmospheric components existing above the cloud layer. The top of the cloud layer is a free parameter for N_2/O_2- and CO_2-rich atmospheres (set to 10 and 30 km, taken from the Earth and Venus, respectively). We treat the case of the N_2/H_2O-rich atmosphere separately because H_2O is a highly condensable species.

2.2.5. Composition, vertical structure and location of the clouds in a N_2/H_2O-rich atmosphere

The temperature gradient of an atmosphere containing non-negligible amount of condensable species, like H_2O, significantly departs from the case where no condensation occurs. A correct estimation of the temperature profile is crucial to determine the scale height, hence the detectability of that atmosphere. In an H_2O-rich atmosphere, the evolution of the adiabatic temperature gradient is driven by the ratio of the partial pressure of water vapor, e, to the saturating vapor pressure, $e_{\rm sat}$. This ratio should also determine the levels at which the water vapor is in excess in the air and condenses (for $e/e_{\rm sat} > 1$), i.e. the levels where clouds may form.

Our initial conditions at the $z = 0$ level (z^0) are the temperature T^0 and pressure p^0. With these quantities we can estimate $e_{\rm sat}$, which depends only on the temperature, using the Clausius-Clapeyron equation:

$$e_{\rm sat}(T) = p^* \exp\left[\frac{\mu_{\rm H_2O} L_v}{\mathcal{N}_A k}\left(\frac{1}{T^*} - \frac{1}{T}\right)\right] \quad (5)$$

where p^* and T^* are the reference pressure ($1.013 \cdot 10^5$ Pa) and temperature (373 K), $\mu_{\rm H_2O}$ is the molar mass of water and L_v is the latent heat of vaporization for water ($2.26 \cdot 10^{10}$ erg g^{-1}). Assuming that the planet is covered with liquid water (e.g., an ocean-planet; see Léger et al. 2004) and that T^0 is 'tropical' (e.g. 340 K), the humidity at the surface is high so that the value of e^0 must be an important fraction of $e_{\rm sat}(T^0)$. We set e^0 to half the value of $e_{\rm sat}(T^0)$. The volume mixing ratio of water can be expressed as $Y_{\rm H_2O} = e/p$, and we can calculate it at the surface of the planet. The atmosphere of an ocean-planet may also contain a significant quantity of CO_2. We arbitrarily set this quantity constant to $Y_{\rm CO_2} = 0.1$ (Léger et al. 2004; Ehrenreich et al. 2005b). Molecular nitrogen is the major constituent of the atmosphere of the Earth and the second more abundant species in the atmosphere of Venus, and therefore we chose to include it to complete the chemical composition of this atmosphere. The mixing ratio of N_2 was set to be $Y_{\rm N_2} = 1 - Y_{\rm CO_2} - Y_{\rm H_2O}$ at any level. Assuming the atmosphere contains only N_2, H_2O and CO_2, we can obtain the mean molar mass of the atmospheric gas ($\mu^0 = \sum_i Y_i^0 \mu_i$) and that of the dry atmospheric gas ($\mu_{\rm d}^0 = \mu^0 - Y_{\rm H_2O}^0 \mu_{\rm H_2O}$), the mean specific heat of dry air ($C_p^0 = \sum C_{p_i} Y_i^0 \mu_i / \mu_{\rm d}^0$) and the scale height H_0 (all at the level z^0).

For the z^{j+1} level, we need to evaluate the temperature gradient between z^j and z^{j+1}. There are two cases (Triplet & Roche 1986):

- $e^j < e_{\rm sat}^j$; in this case the temperature follows a dry adiabatic gradient,

$$\Delta T_{\rm dry} = \frac{-g}{C_p^j}. \quad (6)$$

- $e^j = e_{\rm sat}^j$; in this case the gradient is saturated,

$$\Delta T_{\rm sat} = \Delta T_{\rm dry} \frac{\left(1 + r_{\rm sat}^j\right)\left[1 + L_v r_{\rm sat}^j / (R_{\rm dry}^j T^j)\right]}{1 + \frac{r_{\rm sat}^j}{C_p^j}\left[C_{p_{\rm H_2O}} + L_v^2 \frac{1 + r_{\rm sat}^j R_{\rm H_2O} R_{\rm dry}^j}{R_{\rm H_2O}(T^j)^2}\right]} \quad (7)$$

  where $r_{\rm sat}^j = (\mu_{\rm H_2O} e_{\rm sat}^j)/[\mu_{\rm d}^j (p^j - e_{\rm sat}^j)]$ is the mixing ratio of saturated air, $R_{\rm dry}^j = \mathcal{N}_A k / \mu_{\rm dry}^j$ and $R_{\rm H_2O} = \mathcal{N}_A k / \mu_{\rm H_2O}$ are the specific constant of dry air at the level z^j and water (respectively).

If $z^{j+1} < 20$ km, we select the appropriate gradient accordingly to the value of $e/e_{\rm sat}$, and get the value of the temperature T^{j+1}. Above 20 km, we assume the temperature profile becomes isothermal ($T^{j+1} = T^j$).

The assumption of an isothermal atmosphere, already discussed in Sect. 2.2.2, is somewhat arbitrary but is motivated by an analogy with the atmosphere of the Earth, where the temperature gradient becomes positive from about 20 to 50 km. Taking an isothermal temperature gradient will conservatively mimic the presence of a stratosphere. However, it has important consequences since it allows H_2O to be significantly present above the cloud top. In fact, above 20 km, the temperature stops decreasing, preventing condensation from occurring (the saturation vapor pressure depends only on temperature). Our assumption consequently fixes the height of the cloud deck to the point where the temperature profile is isothermal (actually, one scale height above that point). If we set this point higher, we would increase the amount of clouds hence reducing the detectable portion of atmosphere. In addition, the cloud formation would certainly take the corresponding latent heat of condensation out of the atmospheric gas, contributing, as a consequence, to cool the atmosphere at the level of the cloud layer.

We calculate H^{j+1}, $p^{j+1} = p^j \cdot \exp\left(-z^{j+1}/H^{j+1}\right)$, $e_{\rm sat}^j$ (from Eq. 5) and either $e^{j+1} = e^j \cdot \exp\left[(z^j - z^{j+1})/H^{j+1})\right]$, if the atmosphere is not saturated or $e^{j+1} = e_{\rm sat}^{j+1}$, if the atmosphere is saturated. We finally find all Y_i^{j+1}, $\mu_{\rm dry}^{j+1}$ and $C_{p_{\rm dry}}^{j+1}$ and then iterate the process for all atmospheric levels.

The higher and the lower pressure levels where $e = e_{\rm sat}$ indicate respectively the bottom and the top of the region where clouds are forming. We assume the cloud layer does not extend over one scale height above the top of the cloud forming region. However, we can still have $e \leq e_{\rm sat}$ higher in the atmosphere, and thus H_2O can be present above the clouds.

2.3. Description of atmospheric absorptions

2.3.1. Chemical species

We used the program LBLABC (Meadows & Crisp 1996), a line-by-line model that generates monochromatic gas absorption coefficients from molecular line lists, for each of the gases, except ozone, present in the atmosphere. The line lists are extracted from the HITRAN 2000 databank (Rothman et al. 2003). We calculated the absorption coefficients for O_2, H_2O and CO_2 in our wavelength range we (i.e., from 200 to 2 000 nm).

The absorption coefficients relative to these species depend on pressure and temperature. We verified that those variations do not impact significantly on the results obtained (see Sect. 4) and we decided to use the absorption coefficients calculated at the pressure and temperature of the cloud layer, i.e., 10 km in models A1, A2 & A3, 30 km in models B1, B2 & B3 and from 25 to 70 km in models C1 to C3. We then assumed these absorption coefficients to be constant along the z-axis. This is a fairly good approximation since molecules at that atmospheric level contribute more substantially to the transmitted spectrum than molecules at the bottom of the atmosphere. Absorption coefficients for H_2O, CO_2, O_3 and O_2 are compared in Fig. 5.

The spectrum of O_3 is unavailable in HITRAN at wavelengths lower than 2.4 μm. However it has strong absorption in the Hartley (200–350 nm) and Chappuis (400–750 nm) bands. Thus we took the photo-absorption cross-sections, σ (in cm^2), from the GEISA/cross-sectional databank (Jacquinet-Husson et al. 1999) and converted them into absorption coefficients, A (in cm^2 g^{-1}), such as $A = \sigma \mathcal{N}_A/\mu$, where μ is the molar mass of the component.

As shown in Fig. 6, the pressure and the temperature variations do not have a significant influence over the cross sections/absorption coefficients of O_3. We therefore used the values given for $p = 1$ atm[3] and $T = 300$ K, and set them constant along the z-axis.

2.3.2. Rayleigh diffusion

Light is scattered toward short wavelengths by atmospheric molecules whose dimensions are comparable to λ. Rayleigh diffusion could be an important indicator of the most abundant atmospheric species. Molecular nitrogen, for instance, does not present any noticeable spectroscopic lines between 0.2 and 2 μm. With a transit observation, the presence of a gas without spectroscopic lines like nitrogen in the Earth atmosphere can be indirectly inferred from the wavelength-dependance of the spectrum ratio continuum. Since Rayleigh scattering cross section of CO_2 is high, Venus-like atmospheric signatures should also present an important Rayleigh scattering contribution.

We have therefore estimated these different contributions. The Rayleigh scattering cross section, σ_R, can be expressed in cgs units as: (Bates 1984; Naus & Ubachs 1999; Sneep & Ubachs 2004)

$$\sigma_R(\bar{\nu}) = \frac{24\pi^3\bar{\nu}^4}{n^2}\left(\frac{r(\bar{\nu})^2-1}{r(\bar{\nu})^2+2}\right) \quad (8)$$

where $\bar{\nu} = 1/\lambda$, n is the number density (cm^{-3}) and r is the refractive index of the gas. The total Rayleigh scattering includes weighted contributions from N_2, O_2, CO_2 and H_2O (i.e., $\sigma_R = \sum_i Y_i \sigma_{Ri}$), and so we need all the corresponding refractive indexes. These are found in Bates (1984) and Sneep & Ubachs (2004) for N_2, O_2 and CO_2.[4]

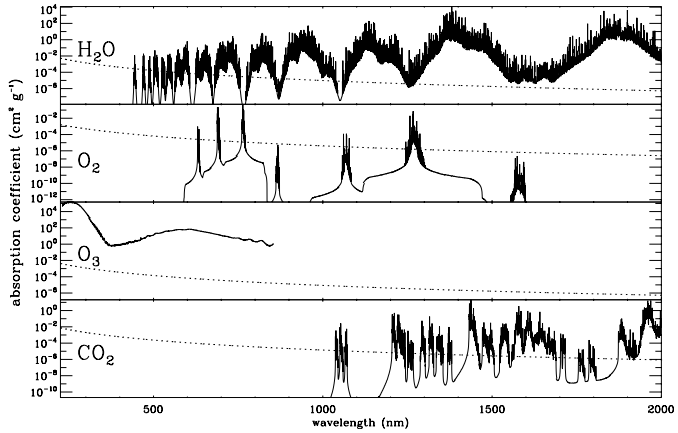

Fig. 5. Absorption coefficients of atmospheric absorbers (in cm^2 g^{-1}), as a function of the wavelength. The photo-absorption coefficients corresponding to H_2O, O_2, O_3 and CO_2 (solid lines) are plotted against their respective Rayleigh scattering coefficient (dotted line), except O_3, plotted against the Rayleigh scattering coefficient of N_2.

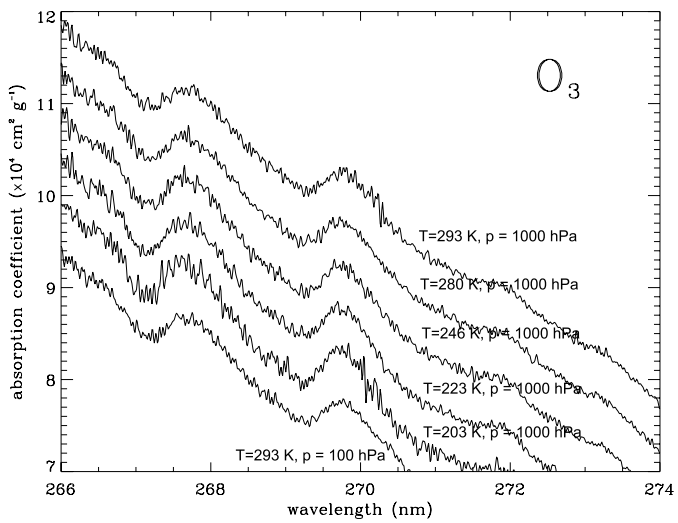

Fig. 6. Dependence of the absorption coefficient of O_3 on pressure and temperature. For clarity, each line has been shifted down by $5{\cdot}10^4$ cm^2 g^{-1} with respect to the previous one.

[3] 1 atm = 1 013 hPa.

[4] We noted a typographical error in the CO_2 refractive index formula (Eq. 13) in Sneep & Ubachs (2004): in order to yield the correct values, results from this expression should be divided by 10^3 (M. Sneep, personal communication).

The refractive index for H_2O comes from Schiebener et al. (1990). Tests have proved the different refractive indexes do not significantly change with temperature and pressure. We have therefore calculated the indexes for standard conditions (15°C and 1013 hPa).

2.3.3. Refraction

Depending on the wavelength, the refraction may bring into the line of sight rays coming from different parts of the star. To quantify the importance of that effect, we calculate the maximum deviation, $\Delta\theta$, due to the wavelength dependence of the refraction index, using the formula given by Seager & Sasselov (2000) and the refractive index at the surface ($h = 0$) between 0.2 and 2 μm. We obtain $\Delta\theta \approx 0.3'$. This represents about 1.5%, 1% and 0.5% of the angular diameter of the star (F-, G- and K-type star, respectively) as seen from the planet. We can therefore consider this effect negligible as long as there are no important variations of the stellar flux on scales lower than the surface corresponding to these numbers.

2.4. Choice of test models

We chose 9 cases, divided into 3 categories: 1 $R_\oplus$-planets (models A1, B1 and C1), 0.5 $R_\oplus$-planets (A2, B2 and C2) and 2 $R_\oplus$-planets (A3, B3 and C3). The parameters for each model are summarized in Table 2. For theses ranges of planetary radii, the depth of the occultation by the tested planets will differ by a factor of ∼16 at most during their transit. Notice that a better detection of the transit itself does not always imply a better detection for the atmosphere of the transiting planet. On the contrary, in some cases, the fainter the transit is, the more detectable the atmosphere will be! In any case, we naturally need to secure the detection of the planet itself before looking for an atmosphere.

The choice of studying planets with a variety of sizes gives us the possibility to explore a large range of planet characteristics, in mass, radius and density. The Earth density is 5.5 $\mathrm{g\,cm^{-3}}$. A planet having the internal composition of the Earth and twice its radius would weigh ∼10 times more, while a planet half large would weigh ∼10 times less (Sotin et al. 2005). That gives densities of 6.1 and 4 $\mathrm{g\,cm^{-3}}$, respectively. We thus have 3 cases, each of which can be coupled with a plausible atmosphere. We chose a N_2/O_2-rich atmosphere (similar to that of the Earth) for models A1, A2 and A3, and a Cytherean (i.e., Venus-like[5]) CO_2-rich atmosphere for models B1, B2 and B3.

Note that the atmospheric pressure profiles are scaled from the 1 $R_\oplus$ cases (A1 and B1) to the 0.5 and 2 $R_\oplus$ models. In doing so, we did not include any species that showed a peak of concentration in altitude, such as the O_3 layer in model A1. In fact, the O_3 peak does not depend only on the hydrostatic equilibrium, but also on the photochemical equilibrium at the tropopause of the Earth. For that reason O_3 is absent in models A2 and A3.

Léger et al. (2004) suggested the existence of 'ocean-planets', whose internal content in volatiles (H_2O) might be as high as 50% in mass. Such planets would be much less dense than telluric ones. We are particularly interested in those ocean-planets since the lower the density of the planet is, the higher the atmosphere extends above the surface. These objects could have densities of 1.8, 2.8 and 4.1 $\mathrm{g\,cm^{-3}}$ for radii of 0.5, 1 and 2 $R_\oplus$ (Sotin et al. 2005), which are relatively small, but reasonable if compared with Titan's density (1.88 $\mathrm{g\,cm^{-3}}$). The huge quantity of water on the surface of an ocean-planet could produce a substantial amount of water vapor in their atmosphere, if the temperature is high enough. A non-negligible concentration of CO_2 might be present as well in those atmospheres (Ehrenreich et al. 2005b). Using this information on ocean-planets, we can simulate three extra cases, namely C1, C2 and C3 (Table 2).

2.5. Choice of different stellar types

In this work, we consider planets orbiting in the habitable zone (HZ) of their parent star. Our atmospheric models are not in fact a good description for planets orbiting too close to their parent star. For instance, the heating of the atmosphere by an extremely close star could trigger effects like evaporation, invalidating the hydrostatic equilibrium we assumed (see, for instance, Lecavelier des Etangs et al. 2004; Tian et al. 2005). The reduced semi-major axis a_r of the orbit of all planets we have considered is defined as:

$$a_r = a \cdot (L_\star/L_\odot)^{-0.5}. \tag{9}$$

We set $a_r = 1$ astronomical unit (AU), so that the planet is in the HZ of its star.

Here we focus on Earth-size planets orbiting around different main sequence stars, such as K-, G- and F-type stars, since the repartition of stellar photons in the spectrum is different from one spectral type to another. Planets in the HZ of K, G and F stars, with $a_r = 1$ AU, should have a real semi-major axis of 0.5, 1 and 2 AU, respectively.

3. Signal-to-noise ratio for ideal observations

Prior to the atmospheres, we need to detect the planets themselves with a dedicated survey, as the one proposed by Catala et al. (2005). The transmission spectroscopy we theoretically study here require the use of a large space telescope. Hence, we need to quantify the S/N of such observations to determine the detectability of the atmospheric signatures for a transiting Earth-size exoplanet. The S/N will depend on both instrumental and astrophysical parameters.

[5] Cythera ($K\acute{\upsilon}\theta\eta\rho\alpha$) is an Ionian island where, according to the Greek mythology, the goddess Aphrodite/Venus first set foot. See `http://en.wikipedia.org/wiki/Cytherean`.

3.1. Instrumental requirements

The first relevant parameter relative to the instrumentation is the effective area of the telescope collecting mirror, S, which can be expressed as $S = (\epsilon D)^2\pi/4$. The coefficient ϵ^2 accounts for the instrumental efficiency and ϵD is thus the 'effective diameter' of the mirror. Up to present, all exoplanetary atmospheric signatures have been detected by the Space Telescope Imaging Spectrograph (STIS) on board the *Hubble Space Telescope (HST)*. This instrument, now no longer operative, was very versatile[6] and consequently not planned to have high efficiency. It had a throughput $\epsilon^2 \approx 2\%$ from 200 to 300 nm, and $\epsilon^2 \approx 10\%$ from 350 to 1 000 nm. As the majority of photons we are interested in is available in the range from 350 to 1 000 nm, we reasonably assume that a modern spectrograph has a mean ϵ^2 significantly greater than 10% from 200 to 2 000 nm. Present day most efficient spectrographs have $\epsilon^2 \approx 25\%$ in the visible, so it seems reasonable to imagine that next generation spectrographs, specifically designed to achieve high sensitivity observations, could have throughput of $\epsilon^2 \approx 25\%$, or $\epsilon = 50\%$.

Another parameter linked to the instrument is the spectral resolution, $\mathcal{R}$. In the following, $\mathcal{R}$ will be assumed to be about 200, i.e. 10 nm-wide spectral feature can be resolved.

Finally, it is legitimate to question the ability of the instrument detectors to discriminate the tenuous ($\sim 10^{-6}$) absorption features in the transmitted spectra of Earth-size planets. In a recent past, sodium was detected at a precision of 50 parts-per-million (ppm) on a line as thin as about 1 nm by Charbonneau et al. (2002) using STIS. According to our results (see Sect. 4), some absorption features from Earth-size planet atmospheres show a ∼1 ppm dimming over ∼100 nm: the technological improvement required to fill the gap should not be unachievable. Besides, since we deal with *relative* measurements – the in-transit signal being compared to the out-of-transit one – there is no need to have detectors with a perfect absolute calibration. Only a highly stable response over periods of several hours is required. Nevertheless, instrumental precision remains a challenging issue whose proper assessment will require further, detailed studies.

3.2. Physical constraints on the observation

The number of photons detected as a function of wavelength depends on the spectral type of the star, while the total number of photons received in an exposure of duration t depends on the apparent magnitude of the star, V. The stellar spectra $F_\star^{V=0}(\lambda)$ are from ρ Capricorni (F2 IV), HD 154 760 (G2 V) and HD 199 580 (K2 IV) and are taken from the Bruzual-Persson-Gunn-Stryker (BPGS) spectrophotometry atlas[7]. The fluxes ($\mathrm{erg\,cm^{-2}\,s^{-1}\,Å^{-1}}$) are given at a null apparent magnitude, so we re-scaled them for any apparent magnitude V, $F_\star = F_\star^{V=0} \cdot 10^{-0.4V}$. The three corresponding spectra are plotted for a default magnitude $V = 8$ in Fig. 7.

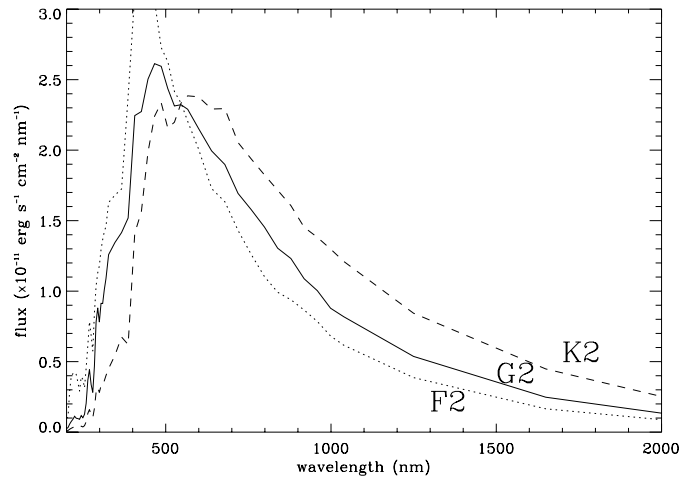

Fig. 7. Spectrum of a K2 (dashed line), G2 (solid line), and F2-type stars (dotted line) between 0.2 and 2 μm. The fluxes are scaled to an apparent magnitude $V = 8$.

The stellar type determines the radius and the mass of the star, so the transit duration (and thus the maximum time of exposure during the transit) is different depending on the star we consider. The transit duration is also a function of the semi-major axis of the planet orbit. Since we chose a constant reduced distance ($a_r = 1$ AU) for all planetary models (see Sect. 2.5), the duration of transit depends on the stellar luminosity as well. From Zombeck (1990), we obtain the radii of F and K stars relatively to that of the Sun, respectively $R_\mathrm{F}/R_\odot \approx 1.25$ and $R_\mathrm{K}/R_\odot \approx 0.75$, the mass ratios, $M_\mathrm{F}/M_\odot \approx 1.75$ and $M_\mathrm{K}/M_\odot \approx 0.5$, and the luminosity ratios, respectively $L_\mathrm{F}/L_\odot \approx 4$ and $L_\mathrm{K}/L_\odot \approx 0.25$. Using Eq. 9, the duration of the transit is:

$$\tau \approx \frac{13\pi}{4}\ \mathrm{h} \cdot \frac{\mathrm{R}_\star}{\mathrm{R}_\odot}\left(\frac{\mathrm{M}_\star}{\mathrm{M}_\odot}\right)^{-0.5}\left(\frac{\mathrm{L}_\star}{\mathrm{L}_\odot}\right)^{0.25}, \qquad (10)$$

where $13\pi/4$ h is the mean transit duration of a planet at 1 AU across a G star averaged over all possible impact parameter of the transit. From Eq. 10 we obtain mean transit durations of 7.6, 10.2 and 13.6 h for K-, G- and F-type star, respectively. In the following, we set $t = \tau$.

Ideally, our observations are limited only by the stellar photon noise – the detection of sodium at a precision of ∼50 ppm in the atmosphere of HD 209 458b by Charbonneau et al. (2002) was in fact limited by the stellar photon noise. However, at the low signal levels we are searching for, the intrinsic stellar noise might need to be considered as well. Stellar activity, as well as convective motions will cause variations in both intensity and color in the target stars, on a large variety of timescales. The impact of stellar micro-variability on the detectability of photometric transits has been addressed by a number of studies (see, e.g., Moutou et al., 2005; Aigrain et al., 2004 – especially their Fig. 8; Lanza et al., 2004), all point-

[6] STIS was used for imagery, spectro-imagery, coronography and low and high resolution spectroscopy.

[7] Available on `ftp.stsci.edu/cdbs/cdbs2/grid/bpgs/`.

ing towards photometric variability levels in the range of ∼100–1 000 ppm for durations of a few days. This is to be compared to the strength and duration of the atmospheric signatures we want to look at: they are ∼1 ppm variations lasting a few hours. While indeed the different time frequency and spectral content of these signatures versus the stellar noise will hopefully allow to discriminate the two, the impact of stellar micro-variability on such faint signals is likely to be significant, and may limit the ability to detect an atmosphere in a transiting planet. For instance, Aigrain et al. (2004) suggested K stars are more adapted than G or F stars regarding to the detection of terrestrial planets versus stellar micro-variability. However, note that the observation of several transits for each planet considered will confirm the signal detected in the first transit. For instance, at $a_r = 1$ AU around a K star, a planet has a period of ≈ 0.3 yr, allowing to schedule several transit observations within a short period of time. Finally, the usual technique to detect a spectral signature from a transit is to compare in-transit and out-of-transit observations (Vidal-Madjar et al. 2003, 2004). For all these reasons, we will assume in the following to be able to discriminate a transit signal from the stellar activity and consequently the photon-noise to be the limiting factor. Nevertheless, further and detailed analysis is certainly needed to quantify the effect of stellar micro-variability, as a function of the stellar type, but this is outside the scope of this paper.

3.3. Calculation of the signal-to-noise ratio

Now let $\varphi_\star$ be the maximum number of photons per element of resolution that can be received during τ: $\varphi_\star = F_\star(\lambda) \cdot \lambda/(h_P c) \cdot \mathcal{R} \cdot S \cdot \tau$, where h_P is Planck's constant and c the speed of light. Some photons are blocked or absorbed by the planet, therefore the actual number of photons received during the transit is $\varphi = \varphi_\star(1 + \Re')$ per element of resolution.

From the observations, it is possible to obtain $\tilde{R}_P$, an estimate of the radius of the transiting planet R_P (e.g., by using the integrated light curve or a fit to the observed spectrum ratio). This value corresponds to the flat spectrum ratio (i.e., a planet without atmosphere) that best fits the data. The corresponding number of photons received during an observation per element of resolution is therefore expressed as: $\tilde{\varphi} = \varphi_\star \left[1 - (\tilde{R}_P/R_\star)^2\right]$.

The weighted difference between φ and $\tilde{\varphi}$ can reveal the presence or the absence of a planetary atmosphere. We express the χ^2 of this difference over all the elements of resolution k as $\sum_k \left[(\varphi_k - \tilde{\varphi}_k)/\sigma_{\varphi_k}\right]^2$. Here, the uncertainty of the number of photons received is considered to be dominated by the stellar photon noise (see Sect. 3.2), that is $\sigma_\varphi = \sqrt{\varphi}$. We thus have:

$$\chi^2 = \sum_k \left(\frac{\varphi_{\star k}}{1 + \Re'_k} \left[\Re'_k + \left(\tilde{R}_P/R_\star \right)^2 \right]^2 \right). \quad (11)$$

Given the χ^2, the S/N can be directly calculated taking its square root. The best estimation can be obtained by minimizing the χ^2 with respect to the radius $\tilde{R}_P$, i.e., $\partial\chi^2/\partial\tilde{R}_P = 0$. From this formula we can calculate the estimated radius:

$$\tilde{R}_P = R_\star \sqrt{-\frac{\sum_k \left[\varphi_{\star k} \Re'_k / \left(1 + \Re'_k\right)\right]}{\sum_k \left[\varphi_{\star k} / \left(1 + \Re'_k\right)\right]}}. \quad (12)$$

Once we determine if an atmosphere is observable or not (depending on the S/N ratio), we can use a similar approach to quantify the detectability of the single atmospheric absorber contributing to the total signal φ. Let $\hat{\varphi}_i = \varphi_\star(1 + \hat{\Re}'_i)$ be the signal obtained by filtering the stellar light out of all atmospheric absorbers except the ith, and let $(\tilde{\hat{\varphi}}_i)$ be its estimation. Here, $\hat{\Re}'_i$ is the spectrum ratio calculated when the species i is not present in the atmosphere. Further, since $(\tilde{\hat{\varphi}}_i) \approx \alpha_i \hat{\varphi}_i$, we can deduce the presence of absorber i in the atmosphere, by simply comparing the fit we made assuming its absence $(\alpha_i \hat{\varphi}_i)$ with the measured signal (φ):

$$\chi_i^2 = \sum_k \left(\frac{\varphi_{\star k}}{1 + \Re'_k} \left[\left(1 + \Re'_k\right) - \alpha_i \left(1 + \hat{\Re}'_{ik}\right) \right]^2 \right), \quad (13)$$

where

$$\alpha_i = \frac{\sum_k \left[\varphi_{\star k} \left(1 + \hat{\Re}'_{ik}\right)\right]}{\sum_k \left[\varphi_{\star k} \left(1 + \hat{\Re}'_{ik}\right)^2 / \left(1 + \Re'_k\right)\right]}. \quad (14)$$

4. Results and discussion

The results of our computations are displayed in Tables 3 & 4 and plotted as spectrum ratios in Figs. 8, 9 & 10.

4.1. Spectral features of interest

Here we summarize the contributions of each atmospheric absorber to the spectrum ratio for various models. The spectral resolution of the plots presented here is 10 nm. The most prominent spectral signatures, when present, are those of O_3 and H_2O. Carbon dioxide is hard to distinguish from H_2O bands and/or its own Rayleigh scattering. Molecular oxygen transitions are too narrow to significantly contribute to the spectrum ratio.

4.1.1. Ozone

In the spectral domain studied here, the Hartley (200–350 nm) and Chappuis (420–830 nm) bands of O_3 appear to be the best indicators of an Earth-like atmosphere. These bands are large (respectively 150 and 600 nm) and lay at the blue edge of the spectrum, where spectral features from other species are missing. There is noticeably no contamination by H_2O, and O_2 strong transitions are narrow and could be easily separated. Ozone bands significantly emerge from Rayleigh scattering and they correspond to very strong transitions, despite the small amount of O_3 present in the model A1 atmosphere ($Y_{O_3} < 10^{-5}$). When present, ozone is more detectable in an atmosphere similar to model A2.

4.1.2. Water

The signature of H_2O is visible in a transit spectrum only if H_2O is substantially abundant above the clouds. This is not the case for models of Earth-like atmosphere like A1, A2 and A3. On the contrary, the models of the ocean-planets (C1, C2 and C3) show a major contribution from this molecule, in the form of four large bands that dominate the red part of the spectrum (at $\lambda \gtrsim 950$ nm). For these three cases, H_2O can be significantly abundant above the clouds.

4.1.3. Carbon dioxide

The lines of CO_2 are about as strongly emerging from the 'continuum' than the H_2O ones, but are often overlapping with these lines. The transitions around 1 600 nm and the ones around 1 950 nm are the easiest to identify, other bands are not observable if water is present. Rayleigh scattering and photo-absorption cross sections of CO_2 are comparable at most wavelengths below 1.8 μm (see Fig. 5), except for a few ∼10-nm wide bands. In fact, the more CO_2 is present in the atmosphere, the more opaque the atmosphere becomes. This implies it would be impossible for an observer on the surface of Venus to see the Sun. Carbon dioxide may be more detectable farther in the infrared, hence making desirable further investigations up to 2.5 μm.

4.1.4. Molecular oxygen

Molecular oxygen does not appear in the plots: its bands at 620, 700, 760 and 1 260 nm are too thin to appear with only 10 nm resolution. Besides, its Rayleigh scattering cross section almost completely masks its absorption features (see Fig. 5) so that no large bands of O_2 can be used as an indicator of its presence. However, note that the presence of O_3 indirectly indicates the presence of O_2, as pointed out by Léger et al. (1993) and others.

4.1.5. Rayleigh scattering

When Hartley and Chappuis bands of O_3 are absent (all cases but A1), the Rayleigh scattering signature is clearly visible in the blue part of the spectrum ratio. On one side it masks the presence of some transitions, like those of O_2 and some of CO_2, but on the other side it can provide two important informations: (i) even if the spectral features cannot be distinguished because they are too thin or faint, the characteristic rising 'continuum' as λ^{-4} for short wavelengths is a clear indication that the planet has an atmosphere, and (ii) it indirectly indicates the presence of the most abundant species of the atmosphere, such as CO_2 and N_2, even if N_2 shows no spectral signature in the observed domain. As a consequence, Rayleigh scattering can be considered a way to detect N_2, provided clouds and/or aerosols do not in turn mask the Rayleigh scattering signature.

To summarize, it is possible to detect the presence of the atmosphere of a transiting exoplanet thanks to the Rayleigh scattering, whatever the composition of the atmosphere is. Moreover, it is theoretically possible to discriminate between an O_2-rich atmosphere, where O_3 is expected to be present (Léger et al. 1993; Sagan et al. 1993) and a H_2O-rich atmosphere, as the O_3 lifetime is supposed to be extremely brief in a water-rich environment. In other words, we should be able to distinguish telluric Earth-like planets with low volatile content from volatile-rich planets. On the other hand, high spectral resolution is needed to discriminate between H_2O-rich planets and Cytherean worlds (B1, B2, B3).

4.2. Parameters influencing the signal-to-noise ratio

4.2.1. Influence of the star

From Table 3 it is clear that the best targets are K-type stars, rather than G- or F-type stars, the former allowing much better S/N than the latter. Two factors are determining the role of the star in the capabilities of detecting an exoplanet atmosphere: (i) The size $R_\star$ of the star, which directly influences the S/N (see Eq. 11) and the duration of transit (Eq. 10) and (ii) the semi-major axis of the planet's orbit, which influences both the duration of transit and the probability to observe the transit from Earth (see below). These factors can explain the discrepancies between the S/N values obtained for different kind of stars in Table 3.

The probability, α, that a planet transiting its parent star might be seen from the Earth is defined as $\alpha \equiv P\{\text{transit}\} = R_\star/a$, with $R_\star$ being the radius of the star and a the semi-major axis of the planet's orbit. This probability is about 10% for 'hot Jupiters', while it is 0.3%, 0.5% and 0.7% for planets orbiting in the HZ of a F, G or K star, respectively.

In addition, K stars are more numerous than other types of stars. From the CDS database, we find there is approximatively a total of $10\,000 \cdot 10^{0.6(V-8)}$ main sequence stars brighter than a given magnitude V on the whole sky.[8] About 3/5 of these are K type stars, against only 1/10 for G stars. Let us now define β to be the number of planet(s) per star, and γ to be the fraction of the sky that is considered for a transit detection survey (in other words the efficiency of surveys to find the targets). We list in Table 4 the number of potential targets for each model. This number, N, corresponds to the number of targets detected with a 10-m telescope mirror effective size and with a S/N greater than or equal to 5. It is given by:

$$N_{\mathrm{S/N}\geq 5,\ \epsilon D=10\,\mathrm{m}} = N_0 \cdot \alpha \cdot \beta \cdot \gamma \cdot \left(\frac{\mathrm{S/N}_{V=8,\,\epsilon D=10\,\mathrm{m}}}{5}\right)^3, \quad (15)$$

where N_0 is about 6 000, 1 000 and 3 000 for K, G and F stars respectively, i.e. the number of stars with magnitude

[8] We consider mostly bright stars, for which the distribution is essentially isotropic.

≥ 8, and $\mathrm{S/N}_{V=8,\,\epsilon D=10\,m}$ is the expected S/N ratio computed for a given atmosphere of a planet orbiting a $V = 8$ star with a telescope having a mirror effective area of 10 m (this value is given in the last column of Table 3). Since no Earth-size planet has been discovered so far, we have no real estimate of β. In the following, when it is not a free parameter we consider $\beta = 1$[9]. Catala et al. (2005) propose a $30° \times 30°$ survey dedicated to find planets around $< 11^{\mathrm{th}}$-magnitude stars, i.e., $\gamma \approx 2$–3% for such a project.

Let be $N_{\mathrm{S/N},\,\epsilon D}$, the number of potential targets reaching a minimum S/N ratio for a given mirror effective size ϵD, which scales from the value calculated using Eq. 15, $N_{\mathrm{S/N}\geq 5,\epsilon D=10\,\mathrm{m}}$, in the following way:

$$N_{\mathrm{S/N},\,\epsilon D} = N_{\mathrm{S/N}\geq 5,\,\epsilon D=10\,\mathrm{m}} \cdot \left(\frac{\mathrm{S/N}}{5}\right)^{-3} \cdot \left(\frac{\epsilon D}{10\ \mathrm{m}}\right)^{3}. \quad (16)$$

The values obtained for atmospheric detection are strongly in favor of a small, late type star. Note that this is also true for the detection of the planetary transit as well.

4.2.2. Effect of the atmospheric temperature gradient

The thick CO_2 Venus-like atmospheres (B1, B2 and B3, see Table 3 & 4) are more difficult to detect than other cases. Even if we set the top of the clouds at 10 km height, the detection remains more challenging than for model A1. That is somewhat surprising, partly because CO_2 has strong transitions, particularly in the near infrared, and partly because of the larger scale height at the surface of the planet (14.3 km for model B1, 8.8 km for model A1). As a consequence, the atmosphere in model B1 should have a larger vertical extent than in model A1. In reality, the difficulty to characterize the atmospheres of models B1, B2 and B3 is related to the temperature profiles we chose (see Fig. 2 and 3): At 50 km of altitude, the temperature of model B1 is roughly 60 K colder than that of model A1. This model in fact benefits from the positive stratospheric temperature gradient of the Earth. Moreover, the atmosphere for model B1 ($\mu_{\mathrm{B1}} = 43\ \mathrm{g\,mol^{-1}}$) is heavier than the one for model A1 ($\mu_{\mathrm{A1}} = 29\ \mathrm{g\,mol^{-1}}$). Therefore, at high altitude, the scale height is larger in model A1 than in model B1 (respectively 7.6 km and 3.9 km at an altitude of 50 km).

4.2.3. Effect of atmospheric pressure

Note that the thickness of the atmosphere in model B1 is almost half the one in A1, despite the intense surface pressure (100 atm), which should help to increase the upper level of the atmosphere, limited by the UV photodissociation ($h_{\max}$). The exponential decrease of pressure prevents, in fact, p_0 to play a key role: in order to counterbalance the effect of the negative temperature gradient, the surface pressure should have been $> 10^6$ atm to obtain absorptions similar to the case of the Earth (model A1).

4.2.4. Effect of the planet gravity and density

The atmospheric absorption is, at a first order, proportional to $H \cdot R_P$. At a given temperature and for a given atmospheric composition, the scale height H is proportional to the inverse of the gravity acceleration, g^{-1}, or equivalently to R_P^2/M_P, where M_P is the mass of the planet. As a result, the absorption is expected to be roughly inversely proportional to the bulk density of the planet, ρ_P, independently of the planet size.

This effect is illustrated by the following examples: models C1, C2 and C3 all benefit from very extended atmospheres, given the weak value of g in the three cases. For a planet as dense as the Earth (such that $g_{\mathrm{C1}} = g_{\mathrm{A1}}$), the results for the N_2/H_2O-rich atmosphere in models C are close to the ones obtained for models A. Both models C and A, present typical spectral features. In model A1, ozone, for which the concentration peaks at the tropopause, gives a prominent signature in the blue edge of the spectral domain (the Hartley and Chappuis bands, as seen in Fig. 8, top panel). On the contrary, the saturated atmosphere of model C1, which sustain H_2O up to high altitudes, yields strong bands around 0.14 and 0.19 μm (Fig. 8, bottom panel). The role played by g can be better understood by comparing model A3 or B3 ($g = 24.5\ \mathrm{m\,s^{-2}}$) to model A2 or B2 ($g = 3.9\ \mathrm{m\,s^{-2}}$), and model C3 ($g = 14.7\ \mathrm{m\,s^{-2}}$) to model C2 ($g = 2\ \mathrm{m\,s^{-2}}$). Using absorption spectroscopy, it is clear that the atmospheres of small and light planets (i.e., with low surface gravity) are easier to detect than the ones of large and dense planets (i.e., with high surface gravity).

Small and light exoplanets, however, may not be able to retain a thick atmosphere. In fact, high thermal agitation of atmospheric atoms causes particles to have a velocity in the tail of the Maxwellian distribution allowing them to escape into space (i.e., Jean's escape). It is therefore questionable if planets of the size of Titan can have a dense atmosphere at 1 AU from their star. Models A2, B2 and C2 enter that category. This problem concerns both small planets and giant exoplanet satellites.

According to Williams et al. (1997), a planet having the density of Mars could retain N and O over more than 4.5 Gyr if it has a mass greater than 0.07 $M_\oplus$. Model planets A2 and B2 have masses of 0.1 $M_\oplus$ and a density equivalent to that of Mars ($\approx$4 $\mathrm{g\,cm^{-3}}$) so they would be able to retain an atmosphere (though they may not be able to have a 1 atm atmosphere, as for Mars). The ocean-planet model C2 has a mass of 0.05 $M_\oplus$ for a density of 2.8 $\mathrm{g\,cm^{-3}}$, and according to Williams et al. (1997), its atmosphere should consequently escape. However, although at 1 AU from the star, such a planet also has a huge reservoir of volatile elements. This reservoir should help to 'refill' the escaping atmosphere.

[9] Actually, $\beta = 2$ in the Solar System because there are two Earth-size planets with atmospheres, namely Venus and the Earth.

Note that an hydrodynamically escaping atmosphere should be easier to detect than a stable one, since it can bring heavier elements into the hot upper atmosphere. This effect is illustrated by the absorptions seen by Vidal-Madjar et al. (2003, 2004) in the spectrum of HD 209 458, which originate in its transiting giant planet hydrodynamically escaping atmosphere. A model of an 'escaping ocean' is studied by Jura (2004). This process would give interesting absorption signatures in the H_2O bands from the lower atmosphere and in the signatures of the photo-dissociation products of H_2O from the upper atmosphere (such as an absorption of Lyman α photons by the hydrogen atom). See detailed discussion in Jura (2004).

5. Conclusion

The vertical extent of the atmosphere is of extreme importance as concerns the detectability of a remote atmosphere by absorption spectroscopy. This tends to favor less dense objects, like giant exoplanet satellites (as would be an 'exo-Titan') or volatile-rich planets (as ocean-planets, theoretically possible but not observed yet). Cytherean atmospheres are the most challenging to detect. Surface parameters, such as surface pressure and temperature, are not crucial. A temperature gradient that becomes positive at few tens of kilometers height (for instance owing to photochemistry) might help the detection. Our results show that late-type stars are better for detecting and characterizing the atmospheres of planets in transit, since they are smaller, more numerous and present a better probability of being transited by a planet.

The strongest signatures of the atmosphere of a transiting Earth-size planet could be those of H_2O (6 ppm in the case of hypothetical ocean-planets), O_3 ($\sim$1–2 ppm) and CO_2 (1 ppm), considering our spectral study from the UV to the NIR (i.e., from 0.2 to 2 μm). The presence of an atmosphere around hundreds of hypothetical 'ocean-planets' (models C) could be detected with a 10–20 m telescope. The atmospheres of tens of giant exoplanet satellites (model A2) could be in the range of a 20–30 m instrument. A 30–40 m telescope would be required to probe Earth-like atmospheres around Earth-like planets (model A1). These numbers suppose that Earth-size planets are frequent and are efficiently detected by surveys.

Finally, planets with an extended upper atmosphere, like the ones described by Jura (2004), hosting an 'evaporating ocean', or the planets in an 'hydrodynamical blow-off state', are the natural link between the planets we have modelled here and the observed 'hot Jupiters'.

Acknowledgements. We warmly thank Chris Parkinson for careful reading and comments that noticeably improved the manuscript, David Crisp for the code `LBLABC` and the anonymous referee for thorough reading and useful comments on the manuscript. G. Tinetti is supported by NASA Astrobiology Institute – National Research Council.

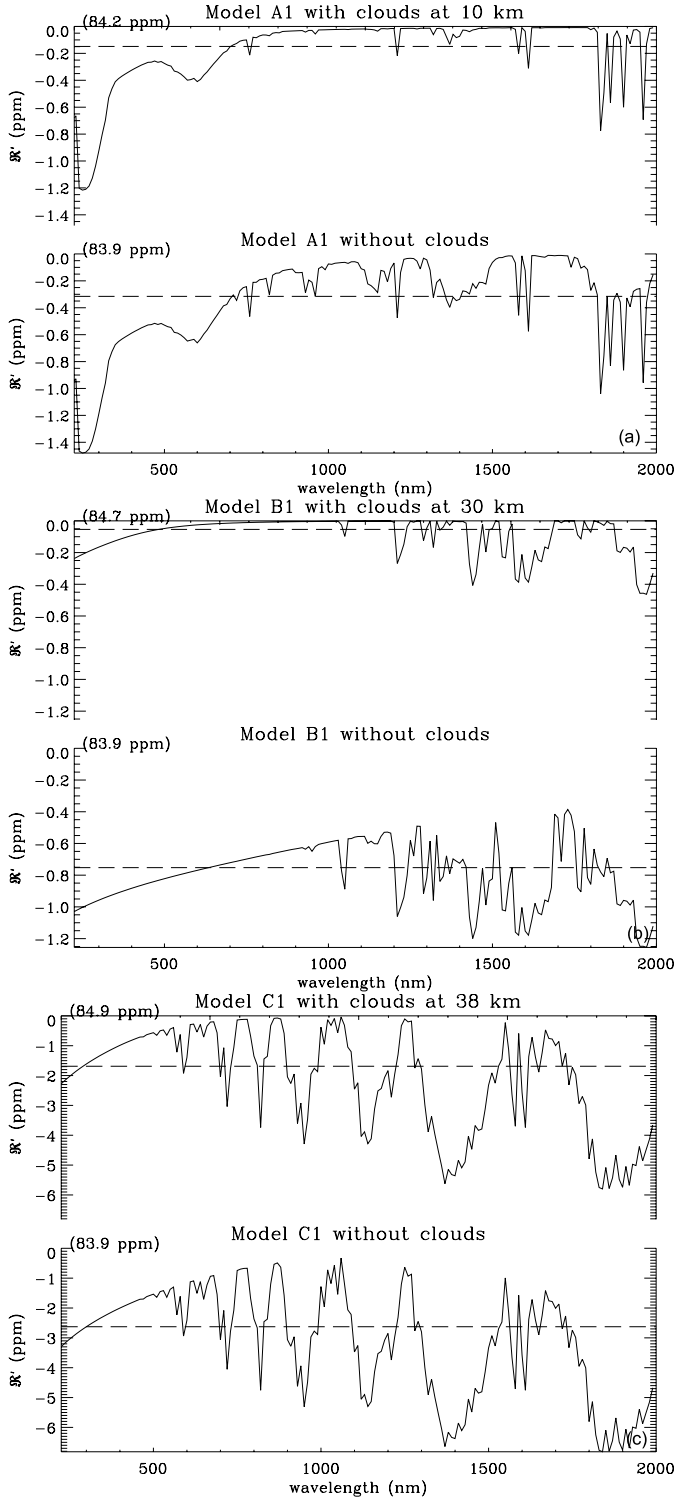

Fig. 8. Spectrum ratios for models A1 (a), B1 (b) and C1 (c). The spectrum ratios have been respectively shifted by the values in parenthesis so that the absorption by the 'solid disk' of the planet is 0 ppm. In the case of models with clouds, the 'solid disk' is artificially increased by the cloud layer. The dashed line indicates the best fit estimation of the radius of the planet, $\tilde{R}_P$ (see Sect. 3) if we suppose there is no atmosphere.

Model	Description	Atm. type	R_P ($R_\oplus$)	M_P ($M_\oplus$)	ρ_P ($g\,cm^{-3}$)	g ($m\,s^{-2}$)	p_0 (atm)	H_0 (km)	h_{max} (km)
A1	(≈)Earth	N_2/O_2-rich	1	1	5.5	9.8	1	8.8	85
B1	(≈)Venus	CO_2-rich	1	1	5.5	9.8	100	14.3	50
C1	medium ocean-planet	N_2/H_2O-rich	1	0.5	2.8	4.9	1	20.0	260
A2	small Earth	N_2/O_2-rich	0.5	0.1	4.0	3.9	1	24.7	260
B2	small Venus	CO_2-rich	0.5	0.1	4.0	3.9	1	40.0	99
C2	small ocean-planet	N_2/H_2O-rich	0.5	0.05	1.8	2.0	1	61.4	499
A3	'super-Earth'	N_2/O_2-rich	2	9	6.1	24.5	1	3.9	30
B3	'super-Venus'	CO_2-rich	2	6	6.1	24.5	100	6.4	30
C3	big ocean-planet	N_2/H_2O-rich	2	9	4.1	14.7	1	6.7	60

Table 2. Summary of test models.

Model	Description	Star	Signal-to-noise ratio $(S/N)_{V=8,\,\epsilon D=10\ m}$					
			w/o cloud	w/ clouds	H_2O	CO_2	O_3	O_2
A1	(≈)Earth	K	5.2	3.5	1.7	1.1	1.9	0.2
		G	3.2	2.3	0.8	0.5	1.2	0.2
		F	2.3	1.7	0.5	0.3	0.9	0.1
B1	(≈)Venus	K	4.0	2.3	0.0	2.3	-	-
		G	2.1	1.2	0.0	1.2	-	-
		F	1.3	0.7	0.0	0.7	-	-
C1	medium ocean-planet	K	41	39	39	11	-	-
		G	22	20	20	5.4	-	-
		F	14	13	13	3.3	-	-
A2	small Earth	K	6.9	6.3	3.8	2.8	-	0.7
		G	4.3	4.0	1.8	1.4	-	0.5
		F	3.2	3.0	1.1	0.8	-	0.3
B2	small Venus	K	5.8	3.3	0.0	3.3	-	-
		G	3.0	1.6	0.0	1.7	-	-
		F	1.9	1.0	0.0	1.0	-	-
C2	small ocean-planet	K	47	46	46	17	-	-
		G	26	25	25	8.6	-	-
		F	17	16	16	5.2	-	-
A3	super-Earth	K	4.6	1.1	0.9	0.5	-	0.1
		G	2.5	0.6	0.4	0.2	-	0.1
		F	1.7	0.4	0.3	0.1	-	0.0
B3	super-Venus	K	5.6	0	0	0	-	-
		G	2.9	0	0	0	-	-
		F	1.9	0	0	0	-	-
C3	big ocean-planet	K	20	13	12	3.2	-	-
		G	10	6.5	6.3	1.5	-	-
		F	6.7	4.1	4.0	0.9	-	-

Table 3. Summary of results: signal-to-noise ratios obtainable with a telescope mirror effective size of $\epsilon D = 10$ m pointing at a $V = 8$ star. To get the S/N ratios for a different effective size ϵD, exposure time during transit, t, and/or apparent magnitude of the star, V, the result scales with $(\epsilon D/10\ \mathrm{m}) \cdot (t/\tau)^{0.5} \cdot 10^{-0.2(V-8)}$ where τ is defined by Eq. 10. The S/N by species are calculated for the models with clouds.

References

Aigrain, S., Favata, F., & Gilmore, G. 2004, A&A, 414, 1139

Bates, D. R. 1984, P&SS, 32, 785

Brown, T. M. 2001, ApJ, 553, 1006

Catala, C., Aerts, C., Aigrain, S., et al. 2005, Proc. 39th ESLAB Symposium, Noordwijk, 19–21 April 2005, Favata F., & Gimenez, A., eds.

Charbonneau, D., Brown, T. M., Latham, D. W., et al. 2000, ApJ, 529, 45

Charbonnneau, D., Brown, T. M., Noyes, R. W., & Gilliland, R. L. 2002, ApJ, 568, 377

Dubois, V. 2002, PhD. thesis, Université de Nantes – Observatoire de Paris

Elliot, J. L., & Olkin, C. B. 1996, ARE&PS, 24, 89

Ehrenreich, D., Despois, D., Léger, A., et al. 2005, in preparation

Fishbein, E., Farmer, C. B., Granger, S. L., et al. 2003, IEEE Transactions on Geoscience and Remote Sensing, 41, 2

Green, D., Matthews, J., Seager, S., & Kuschnig, R. 2003, ApJ, 597, 590

Hubbard, W. B., Fortney, J. J., Lunine, J. I., et al. 2001, ApJ, 560, 413

Model	Description	Star	Mirror eff. size (m) $(\epsilon D)_{\mathrm{S/N}\geq 5,\, V=8}$ w/ clouds	Limiting magnitude $(V_{\mathrm{Lim}})_{\mathrm{S/N}\geq 5,\, \epsilon D=10\,\mathrm{m}}$ w/ clouds	Number of stars	Number of targets for models w/ clouds $(N)_{\mathrm{S/N}\geq 5},\ \epsilon = 50\%$ $\beta\cdot\gamma = 1$ $D = 20$ m	$\beta\cdot\gamma = 3\%$ D = 30 m	$\beta\cdot\gamma = 10\%$ $D = 30$ m
			(a)	(b)	(c)	(d)		
A1	(≈)Earth	K	14	7.22	2 042	14	1	4
		G	22	6.31	96	< 1 (0.4)	$\ll 1$	< 1 (0.1)
		F	29	5.66	118	< 1 (0.3)	$\ll 1$	< 1 (0.1)
B1	(≈)Venus	K	21	6.31	580	4	< 1 (0.4)	1
		G	43	4.90	13	$\ll 1$	$\ll 1$	$\ll 1$
		F	68	3.73	8	$\ll 1$	$\ll 1$	$\ll 1$
C1	medium ocean-planet	K	1.3	12.5	$> 3\cdot 10^6$	19 602	1 984	6 615
		G	2.5	11.0	63 095	321	32	108
		F	3.9	10.1	54 591	157	15	52
A2	small Earth	K	8	8.50	11 971	84	8	28
		G	13	7.51	508	2	< 1 (0.2)	< 1 (0.6)
		F	17	6.90	656	1	< 1 (0.1)	< 1 (0.3)
B2	small Venus	K	15	7.10	1 730	12	1	4
		G	31	5.52	32	< 1(0.1)	$\ll 1$	$\ll 1$
		F	50	4.50	23	$\ll 1$	$\ll 1$	$\ll 1$
C2	small ocean-planet	K	1.1	12.8	$> 4\cdot 10^6$	33 569	3 398	11 329
		G	2.0	11.5	125 892	600	60	202
		F	3.1	10.5	94 868	307	31	103
A3	super-Earth	K	45	4.71	63	< 1 (0.4)	$\ll 1$	< 1 (0.1)
		G	86	3.39	1	$\ll 1$	$\ll 1$	$\ll 1$
		F	121	2.51	1	$\ll 1$	$\ll 1$	$\ll 1$
B3	super-Venus	K	$> 10^3$	-	0	$\ll 1$	$\ll 1$	$\ll 1$
		G	$> 10^3$	-	0	$\ll 1$	$\ll 1$	$\ll 1$
		F	$> 10^3$	-	0	$\ll 1$	$\ll 1$	$\ll 1$
C3	big ocean-planet	K	4.0	10.1	109 182	682	69	230
		G	7.7	8.57	2 197	10	1	3
		F	13	7.57	1 656	4	< 1 (0.4)	1

Table 4. Summary of results: mirror effective size and number of targets.
(a) Effective size $(\epsilon D)_{\mathrm{S/N}\geq 5,\, V=8}$ of the telescope mirror required to obtain S/N = 5 for a $V = 8$ star, based on the numbers displayed for the models with clouds (see Table 3).
(b) The limiting magnitude at which the number of targets in the last column is given. This can be expressed as $(V_{\mathrm{Lim}})_{\mathrm{S/N}\geq 5,\, \epsilon D=10\,\mathrm{m}} = 5\cdot\log_{10}\left[\left(\mathrm{S/N}_{V=8,\, \epsilon D=10}\right)/5\cdot(\epsilon D)/10\ \mathrm{m}\right] + 8$.
(c) Total number of given spectral-type stars brighter than the limiting magnitude.
(d) Number of potential targets calculated with Eq. 15, using the S/N value of the models with clouds and assuming various $\beta\cdot\gamma$ values. The coefficients β and γ are defined in the text. When the number of potential targets is slightly less than 1, the value is given between parenthesis. Use Eq. 16 to scale the value displayed in the column to any mirror effective size ϵD and minimum S/N.

Jacquinet-Husson, N., Arié, E., Ballard, J., et al. 1999, JQSRT, 62, 205
Jura, M. 2004, ApJ, 605, 65
Kasting, J. F., Whitmire, D. P., & Reynolds R. T. 1993, Icarus, 101, 108
Kliore, A. J., Moroz, V. I., & Keating, G. M. 1985, eds., Adv. Space Res., 5, 11, 1
Henry, G. W., Marcy, G. W., Butler, R. P., et al. 2000, ApJ, 529, 41
Lanza, A. F., Rodonò, M., & Pagano, I. 2004, A&A, 425, 707
Lecavelier des Etangs, A., Vidal-Madjar, A., McConnell, J. C., & Hébrard, G. 2004, A&A, 418, 1
Léger, A., Pirre, M., & Marceau, F. J. 1993, A&A, 277, 309
Léger, A., Selsis, F., Sotin, C., et al. 2004, Icarus, 169, 499
Mazeh, T., Naef, D., Torres, G., et al. 2000, ApJ, 532, 55
McArthur, B. E., Endl, M., Cochran, W. D., et al. 2004, ApJ, 614, 81
Meadows, V. S., & Crisp, D. 1996, JGR, 101, 4595
Moutou, C., Pont, F., Barge, P., et al. 2005, A&A, 437, 355
Naus, H., & Ubachs, W. 2000, Optics Letters, 25, 347
Rivera, E., Lissauer, J., Butler, P., et al. 2005, submitted to ApJ Letters
Rothman, L. S., Barbe, A., Benner, D. C., et al. 2003, JQSRT, 82, 5
Sagan, C., Thomson, W. R., Carlson, R., et al. 1993, Nature, 365, 715
Santos, N. C., Bouchy, F., Mayor, M., et al. 2004, A&A, 426, 19
Sato, B., Fischer, D. A., Henry, G. W., et al. 2005, ApJ, in press, astro-ph/0507009

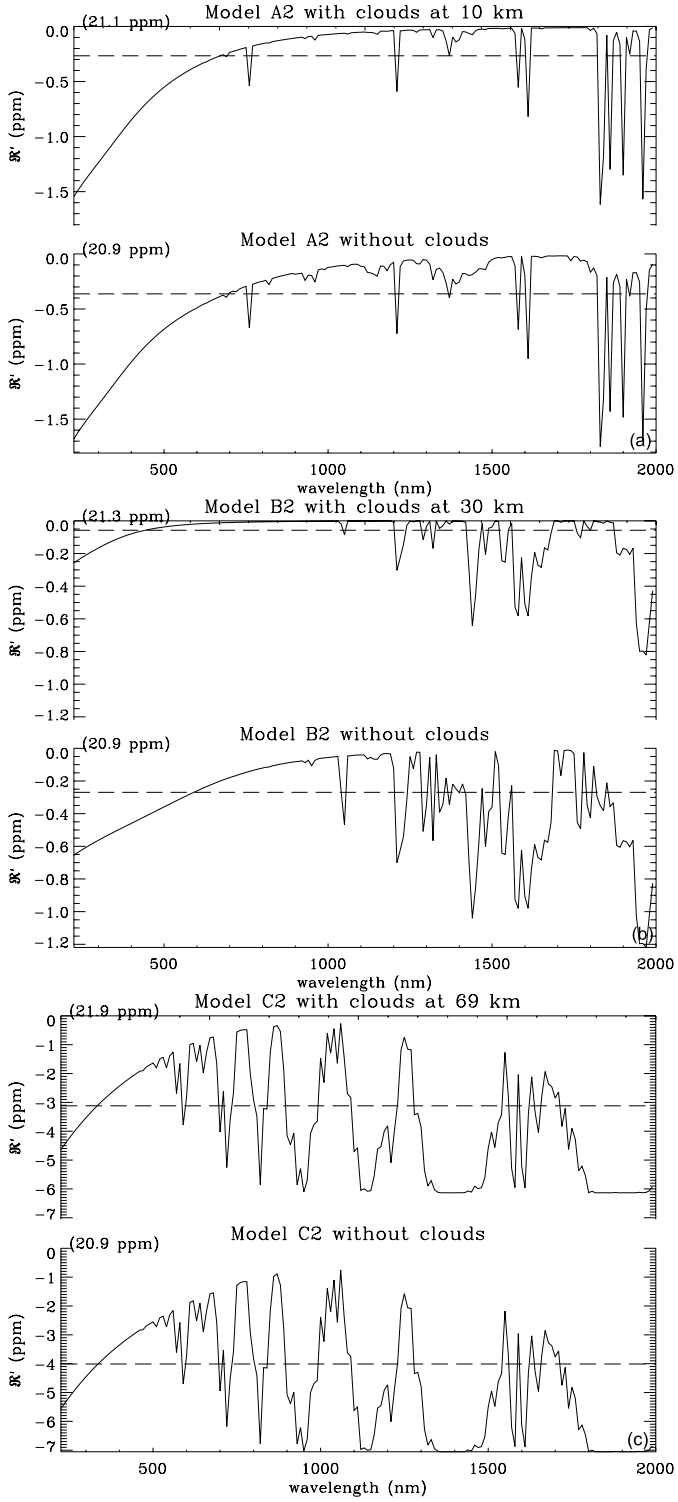

Fig. 9. Spectrum ratios for models A2 (a), B2 (b) and C2 (c). The 'saturation effect' in H_2O lines, for model C2, is a consequence of the atmosphere being optically thick at the upper atmospheric level, $h_{\max}$. In fact, if one consider there is no more water above this level due to photodissociation (see Sect. 2.2.3), such transmitted spectrum plots allow to determine the level where H_2O photodissociation occurs in an exoplanet atmosphere.

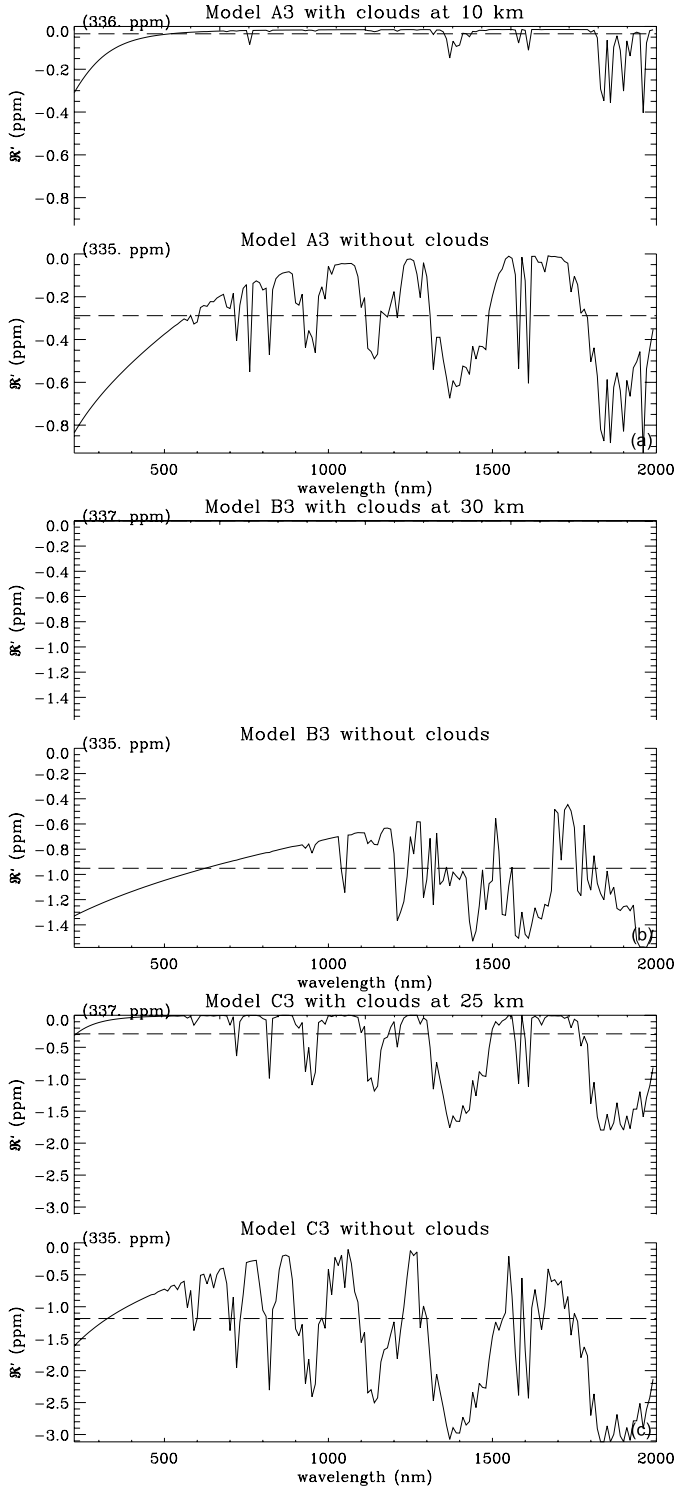

Fig. 10. Spectrum ratios for models A3 (a), B3 (b) and C3 (c).

Schiebener, P., Straub, J., Levelt Sengers, J. M. H., et al. 1990, J. Phys. Chem. Ref. Data, 19, 677

Seager, S., & Sasselov, D. 2000, ApJ, 537, 916

Segura, A., Krelove, K., Kasting, J. F., et al. 2003, Astrobiology, 3, 689

Sneep, M., & Ubachs, W. 2005, JQSRT, 92, 293

Sotin, C., et al. 2005, submitted to A&A

Tian, F., Toon, O. B., Pavlov, A. A., et al. 2005, ApJ, 621, 1049
Tinetti, G., Meadows V. S., Crisp D., et al. 2005, Astrobiology, 5, 461
Tinetti, G., Meadows V. S., Crisp D., et al. 2005, submitted to Astrobiology, astro-ph/0502238
Triplet, J.-P., & Roche, G. 1986, Météorologie générale, ed. Météo France, 3rd edition
Vidal-Madjar, A., Lecavelier des Etangs, A., Désert, J.-M., et al. 2003, Nature, 422, 143
Vidal-Madjar, A., Désert, J.-M., Lecavelier des Etangs, A., et al. 2004, ApJ, 604, 69
Williams, D. M., Kasting, J. F., & Wade, R. A. 1997, Nature, 385, 234
Wolszczan, A. & Frail, D. A. 1992, Nature, 355, 145
Zombeck, M., V. 1990, Handbook of space astronomy & astrophysics, Cambridge University Press, 2nd edition